MECHANICALLY-TUNABLE METAMATERIAL FOR MULTI-BAND ABSORPTION

Duong Thi Ha[1,3], Bui Xuan Khuyen[1,2*], Bui Son Tung[1,2], Pham Thanh Son[2], Vu Thi Hong Hanh[3], Trinh Thi Giang[2], Nguyen Thanh Tung[1,2], Vu Dinh Lam[1]
[1]Graduate University of Science and Technology - VAST,
[2]Institute of Materials Science - VAST, [3]TNU - University of Education

ARTICLE INFO

Received: 31/8/2023
Revised: 03/11/2023
Published: 03/11/2023

KEYWORDS

Metamaterial perfect absorber
Mechanically-tunable
Multi-band absorption
THz region
Flexible metamaterial

ABSTRACT

In this work, we proposed a mechanically-tunable metamaterial perfect absorber by exploiting a pasted nano silver ink on flexible polyimide substrate. At flat configuration, the proposed structure is acted as a single band metamaterial absorber in which a resonance peak induced at 3.7 GHz with an absorptivity of 99.9%. Under mechanical deformation, our structure is bent and wrapped on to a cylindrical surface. At this configuration, the high absorption feature at 3.7 GHz is maintained well while there are new peaks appear at higher frequencies. When the bending radius changes from 400 mm to 200 mm, the proposed structure can be switched between single-band and triple-band models. In addition, the designed MPA exhibits polarization-insensitive and stable with respect to the oblique incidence up to 50 degrees. Furthermore, for both flat and curved states, the absorption mechanism is explained by the perfect impedance matching and the surface current distributions. Finally, the design of the MPA is scaled down for operation in the THz region, while still demonstrating effective tunability between single-band and dual-band absorption modes through mechanical deformation.

VẬT LIỆU BIẾN HÓA CÓ KHẢ NĂNG ĐIỀU KHIỂN CƠ HỌC CHO HẤP THỤ ĐA BĂNG TẦN

Dương Thị Hà[1,3], Bùi Xuân Khuyến[1,2*], Bùi Sơn Tùng[1,2], Phạm Thanh Sơn[2], Vũ Thị Hồng Hạnh[3], Trịnh Thị Giang[2], Nguyễn Thanh Tùng[1,2], Vũ Đình Lãm[1]
[1]Học viện Khoa học và Công nghệ - Viện Hàn lâm Khoa học và Công nghệ Việt Nam
[2]Viện Khoa học vật liệu - Viện Hàn lâm Khoa học và Công nghệ Việt Nam, [3]Trường Đại học Sư phạm - ĐH Thái Nguyên

THÔNG TIN BÀI BÁO

Ngày nhận bài: 31/8/2023
Ngày hoàn thiện: 03/11/2023
Ngày đăng: 03/11/2023

TỪ KHÓA

Vật liệu biến hóa hấp thụ tuyệt đối sóng điện từ
Khả năng điều khiển cơ học
Hấp thụ đa băng tần
Vùng THz
Vật liệu biến hóa đàn hồi

TÓM TẮT

Trong nghiên cứu này, chúng tôi đã đề xuất một vật liệu biến hóa hấp thụ tuyệt đối sóng điện từ có thể điều khiển bằng tác động cơ học bằng cách sử dụng mực nano bạc in lên trên đế polyimide đàn hồi. Ở cấu hình phẳng, cấu trúc đề xuất hoạt động như một vật liệu biến hóa hấp thụ một băng tần với một đỉnh hấp thụ tại tần số 3,7 GHz và độ hấp thụ đạt tới 99,9%. Dưới tác động cơ học, cấu trúc được uốn cong và bọc lên trên một bề mặt hình trụ. Ở cấu hình này, đỉnh hấp thụ tại tần số 3,7 GHz vẫn được duy trì tốt trong khi có những đỉnh hấp thụ mới xuất hiện ở vùng tần số cao hơn. Khi bán kính uốn thay đổi từ 400 mm đến 200 mm, cấu trúc đề xuất có tính năng chuyển đổi được giữa chế độ hấp thụ một băng tần và hấp thụ ba băng tần. Ngoài ra, vật liệu biến hóa hấp thụ tuyệt đối sóng điện từ được thiết kế thể hiện đặc tính không nhạy với sự phân cực của sóng tới và ổn định đối với góc tới lên tới 50 độ. Hơn nữa, đối với cả trạng thái phẳng và trạng thái cong, cơ chế hấp thụ được giải thích bằng sự phối hợp trở kháng và phân bố dòng điện bề mặt. Cuối cùng, thiết kế của vật liệu biến hóa hấp thụ tuyệt đối sóng điện từ được thu nhỏ lại để hoạt động ở vùng THz, đồng thời vẫn thể hiện khả năng điều chỉnh hiệu quả giữa chế độ hấp thụ một băng tần và hai băng tần thông qua tác động cơ học.

DOI: https://doi.org/10.34238/tnu-jst.8659

* Corresponding author. *Email: khuyenbx@ims.vast.ac.vn*

1. Introduction

Metamaterials (MMs) are artificial materials comprised of periodic structures that exhibit the unit-cell dimensions smaller than the operational wavelength. The effective permittivity and permeability of these metamaterials can be tailored by independently manipulating the structural parameters. This manipulation gives rise to unique electromagnetic properties that are absent in natural materials, such as negative refractive index [1], backward Cherenkov radiation [2], and inverse Doppler effect [3]. Although initially theorized by Veselago in 1968 [4], MMs gained substantial scientific interest and underwent comprehensive investigation only after their experimental validation by Smith in 2000 [5]. Since then, these materials have been extensively explored across a wide spectrum of applications, encompassing sensors [6] – [8], super lenses [9], wireless power transfer [10], [11], and more.

In recent years, a significant avenue of research within the realm of metamaterials has focused on metamaterial perfect absorbers (MPAs), a concept first introduced by Landy et al. in 2008 [1]. Boasting remarkable advantages in terms of absorption efficiency, cost-effectiveness, and reduced thickness compared to traditional absorbers, MPAs have garnered significant attention and have emerged as prospective candidates for diverse applications. These encompass but are not limited to energy harvesting [12], [13], radar cross-section reduction [14], [15], and chemical as well as biomedical sensing [6], [16], [17], among others.

In general, MPA exhibits a structural configuration characterized by three layers: two metal layers separated by a dielectric layer. The upper metal layer encompasses resonant structures which serve the purpose of impedance matching, a requisite condition for achieving perfect absorption. The absorption characteristics of these MPAs predominantly hinge upon their geometric parameters. Consequently, it is imperative to acknowledge that the operational frequency of the MPA cannot be altered subsequent to its fabricationThis limitation assumes considerable significance, particularly within contemporary electronic and electromagnetic systems, wherein the integration of active and reconfigurable controllable devices holds pivotal significance.

Recent efforts have witnessed the introduction of various methodologies aimed at realizing tunable MPAs. These methods encompass the utilization of magnetic fields [19], [20], thermal sources [21], electric fields [22], and liquid crystals [18], among others. While the effectiveness of these techniques in achieving tunable MPAs has been demonstrated, they necessitate intricate fabrication processes. In response to this limitation, the concept of achieving tunable MPAs through mechanical deformation of the absorber structure has emerged. Notably, in 2015, a metamaterial absorber that exhibited both mechanical stretchability and tunability was reported. This absorber was constituted by stacking a dielectric resonator on top of a thin conductive rubber layer [23]. Through the application of stretching forces along the H field, the absorption frequency transitioned from 11.15 GHz to 11.56 GHz. Expanding upon this premise, Kim et al. proposed a mechanically actuated frequency-reconfigurable MPA, characterized by a structural configuration encompassing an air substrate possessing adjustable thickness. Experimental validation substantiated that alteration in the air thickness from 17 mm to 26 mm, achieved through mechanical manipulation, induced a change in the absorption frequency from 6.96 GHz to 5.78 GHz [24]. Moreover, Pham et al. introduced a MM inspired by origami building blocks, capable of being modulated through mechanical stimuli. The proposed versatile characteristics of MM enable its transformation from an ultra-broadband absorber to a reflector, facilitated by manipulation of its folding states [25].

Within the scope of this investigation, we introduce an approach involving a mechanically tunable MPA, leveraging the integration of a flexible polyimide substrate and nano silver ink. In its planar configuration, the devised structure effectively functions as a single-band perfect absorber within the S band frequency range. Remarkably, upon undergoing controlled bending

onto a cylindrical surface with an appropriate radius, the structure's characteristics transform, leading to the emergence of a multi-band absorption phenomenon. Notably, the fundamental absorption peak retains its integrity, exhibiting near-unity absorption. Furthermore, the mechanism of multi-band absorption is also elucidated by investigating the induced currents on the MPA. Crucially, through orchestrated manipulation of curvature states, the proposed MPA configuration exhibits the capacity to transition seamlessly from its original single-band absorber state to a multi-band absorber, thereby introducing an effective way of versatility and control to the realm of metamaterial absorber design. Finally, by scaling down the suggested structure, we obtained a mechanically-tunable MPA operating in the THz range, in which the proposed MPA can be adjusted from single-band to dual-band absorber by mechanical deformation.

2. Design, simulation and experiment

The unit cell schematic of the proposed metamaterial perfect absorber (MPA) is depicted in Figure 1(a), encompassing a tri-layered structure. The uppermost layer is composed of a periodic arrangement of octagonal ring-shaped structures, fabricated from nano-silver ink boasting a conductivity of 10^7 S/m and a thickness measuring 0.035 mm. These octagonal rings possess specific dimensions, with outer and inner radii of r_1 = 8.5 mm and r_2 = 7.5 mm, respectively, which have been meticulously optimized to ensure impedance matching with the surrounding free space. In order to facilitate mechanical reconfigurations while preserving the structural integrity, the dielectric layer is fashioned from polyimide, characterized by a dielectric constant of 3.5 and a loss tangent of 0.0025. The thickness of this dielectric layer, denoted as *t*, has undergone optimization to achieve a value of 0.5 mm. Concluding the assembly, the lower metallic layer is constructed using copper and measures 0.035 mm in thickness.

In this study, simulations were conducted utilizing the CST Microwave Studio software [26]. For the scenario involving normal incidence, the direction of electromagnetic wave, represented by the wavevector k, was aligned parallel to the axis of the ring-shaped structure, while the E-H plane was perpendicular. The boundary conditions were defined as unit cells in the x- and y-directions (E-H plane) and open in the z-direction. The key simulation outcomes comprised the scattering parameters S_{11} and S_{21}. Absorption, denoted as A(ω), was calculated using the formula: $A(\omega) = 1 - R(\omega) - T(\omega)$, where $R(\omega) = |S_{11}|^2$ represents reflection and $T(\omega) = |S_{21}|^2$ represents transmission. Notably, in the specific configuration of our structure, the bottom layer, constituted of a continuous copper plane, effectively eliminated transmittance ($T(\omega) = 0$)). Consequently, the absorption can be simplified to $A(\omega) = 1 - R(\omega) = 1 - |S_{11}|^2$.

The proposed structure was realized through the application of the screen stencil method. The chosen nano silver ink was a commercial product with conductivity of 10^7 S/m, while the substrate adopted was a copper-coated polyimide board. To imprint the patterns onto the polyimide substrate, a stencil was crafted, bearing the octagon array patterns, which was then placed onto the substrate. Subsequently, the nano silver ink was transferred to the substrate through a spraying process, as depicted in Figure 1(b). Finally, the stencil was removed, leaving behind the intended patterns on the polyimide substrate. The completed MPA was visually captured in Figure 1(c).

To assess the absorption performance of the fabricated sample, the electromagnetic response was measured utilizing a vector network analyzer R&S ZNB20. The experimental setup is illustrated in Figure 1(d). The setup entailed the connection of two horn antennas to the analyzer, where one antenna served as the transmitter and the other as the receiver. As a result of the continuous metallic plane at the bottom, only the reflection component was measurable, while transmission was disregarded.

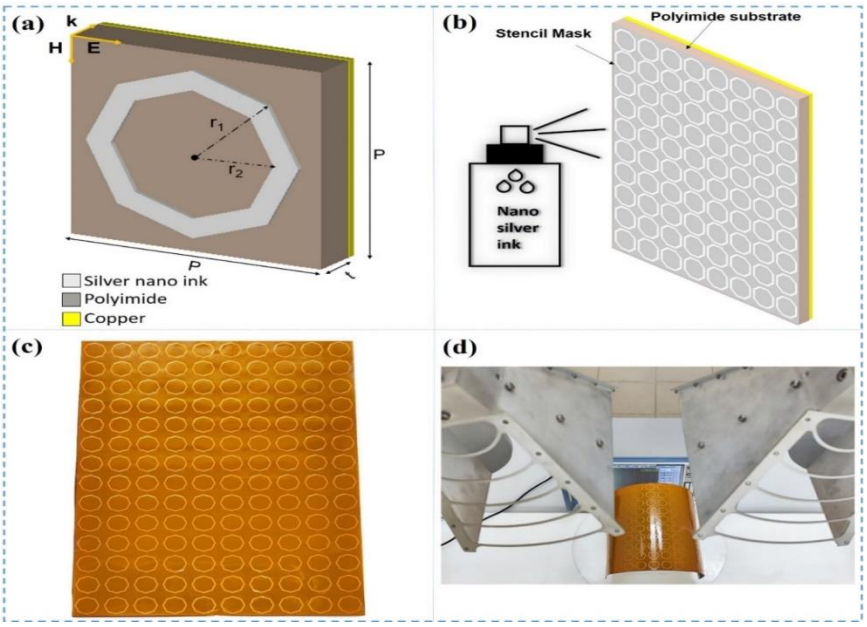

Figure 1. *(a) Schematic of a unit cell of the proposed structure, (b) schematic of fabricated process, (c) fabricated MPA and (d) measurement configuration*

3. Results and discussion

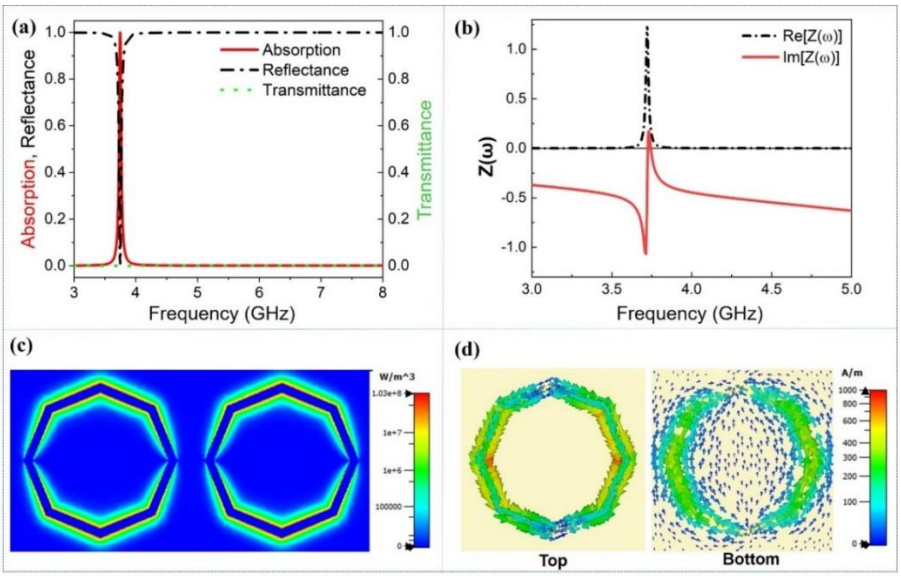

Figure 2. *(a) Simulated absorption, reflection and transmission, (b) effective impedance of the proposed MPA, (c) power loss density and (d) surface currents at 3.7 GHz*

Figure 2(a) shows the simulated absorption, reflection, and transmission spectra of the flat configuration under TE-polarized electromagnetic wave. In this simulation, the electromagnetic wave propagates along the z axis, which is perpendicular to the surface of the structure. It is evident that at 3.7 GHz, both reflectance and transmittance are simultaneously zero, leading to an absorption peak near unity. The absorption mechanism can be elucidated using impedance matching theory. The effective impedance of proposed structure is calculated and presented in Figure 2(b). At 3.7 GHz, the real part of the impedance is 1.009 and its imaginary part is zero. The obtained result demonstrates that the impedance matching condition is satisfied at 3.7 GHz.

Consequently, the electromagnetic wave propagates through the interface between the air and the MPA without being reflected back into the free space. Subsequently, the electromagnetic wave energy is mainly dissipated in the dielectric layer, as depicted in the power loss density distribution shown in Figure 2(c).

To gain insights into the origin of this absorption peak, we simulated the surface current distribution, as presented in Figure 2(d). It can be seen that at 3.7 GHz, the surface currents on the two metallic surfaces are anti-parallel, forming a magnetic dipole. The observed phenomenon indicates the excitation of strong magnetic resonance at 3.7 GHz, which gives rise to the absorption peak [1].

Additionally, the performance of MPA under oblique incidence and different polarization angles was investigated. The influence of polarization angle on the absorption is illustrated in Figure 3(a). Obviously, due to the symmetry of the proposed structure, the absorption spectrum is independent of polarization. Figure 3(b) presents the influence of incident angle on absorption spectrum for the case of TE polarization. It can be observed that, when the incident angle increases from 0° to 60°, the fundamental peak at 3.7 GHz remains above 80%. Moreover, a new peak appears at 7.5 GHz under the oblique incidence. This newly emerged peak achieves the highest absorption of 62.6% when the incident angle is 50°. For TM polarization, the absorption of fundamental peak at 3.7 GHz remains nearly unchanged when the incident angle goes up to 70° and a new peak appears at 7.5 GHz, similar to TE polarization. However, the absorption of this new peak reaches 99% when the incident angle increase to 70^o (Figure 3(c)).

To elucidate the origin of these new peaks, the surface current distributions were simulated for both TE and TM polarizations. Figure 4 shows the simulated surface current distributions at frequency of 7.5 GHz. It can be seen that the surface currents are divided into two regions, with the surface currents on neighboring regions are anti-parallel. Furthermore, there are two current loops, which are anti-parallel between the top and bottom metallic layers [28,29]. Therefore, the observation suggests that the new peak at higher frequency originates from a second-order magnetic resonance.

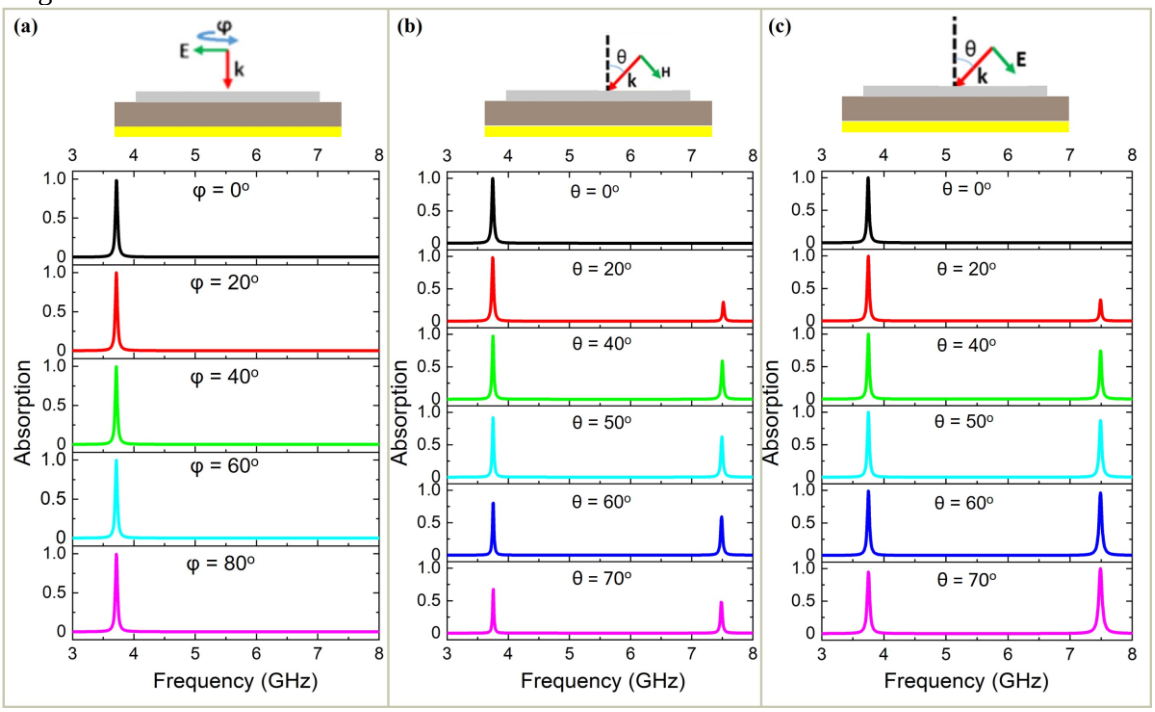

Figure 3. *Absorption spectrum of MPA (a) depends on the the polarization angle, absorption spectrum of MPA depends on the incident angle for (b) TE and (c) TM polarizations*

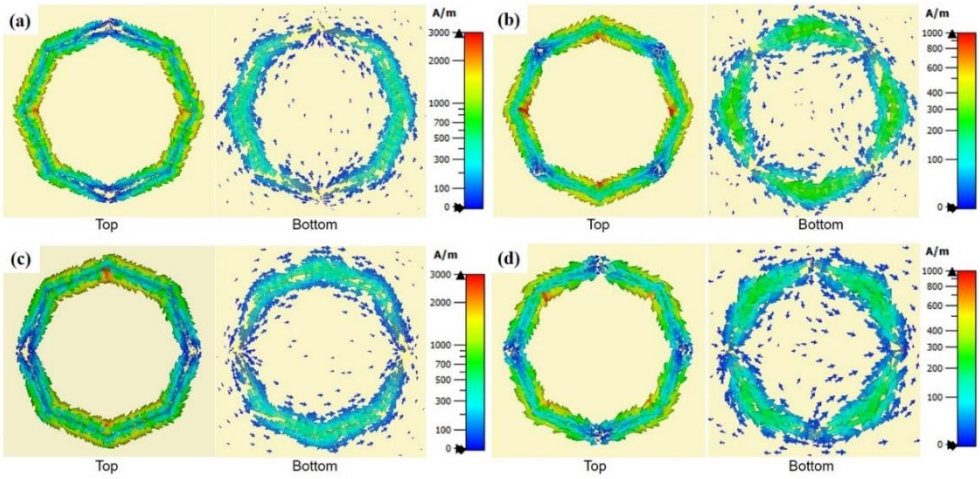

Figure 4. *Surface current distributions on the top and bottom metallic layers for TE polarization at (a) 3.7 GHz, (b) 7.5 GHz and for TM polarization at (c) 3.7 GHz, (d) 7.5 GHz*

Our MPA is designed with a polyimide dielectric known for its excellent flexibility. The selected material enables easy bending and coverage on cylindrical surfaces with varying radii. To evaluate the mechanical tunability of the proposed MPA, we simulated and measured the absorption while MPA was bent to different radii of 400 mm, 300 mm and 200 mm. For the simulation, we constructed a full structure of MPA and the plane-wave propagation was maintained along the z-direction. In the bent state, we focused solely on investigating the absorption performance of MPA under the TE-polarized wave, in which the electric and magnetic fields are oriented along the y- and x-direction, respectively. Figure 5 depicts the bending configuration and defines the bending radius *R*.

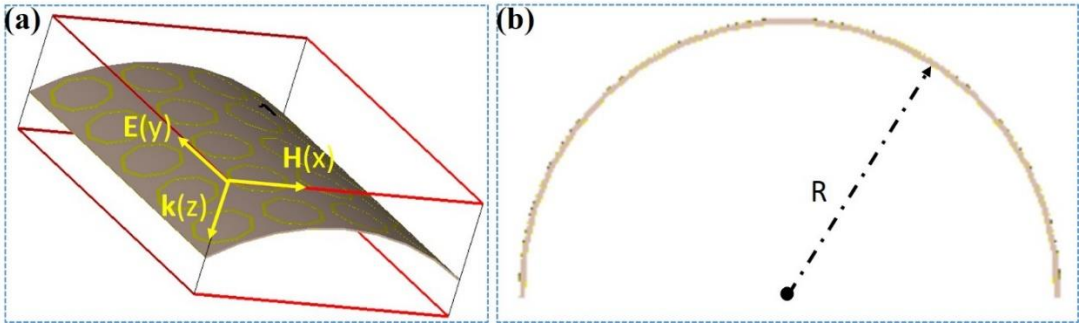

Figure 5. *(a) Bending configuration and (b) bending radius R of the MPA*

Simulation and experiment results of the absorption spectrum with different bending radii are presented in Figure 6. It can be observed that as the proposed MPA changes from flat to bending configuration with various bending radii, the fundamental peak is nearly unchanged for both simulation and experiment (absorption of 99% around 3.7 GHz). However, two new peaks emerge at higher frequencies. Particularly, when *R* decreases to 400 mm, there are two induced peaks in simulation (absorption of 69% and 41% at 7.43 GHz and 7.6 GHz, respectively) and experiment (absorption of 69% at 7.26 GHz and 40.8% at 8.0 GHz). With further reduction in *R* to 300 mm, high-absorption peaks are achieved at 7.43 GHz (92.6%) and 7.6 GHz (65%) in simulation, and at 7.2 GHz (91%) and 7.9 GHz (64.1%) in experiment. However, when *R* drops to 200 mm, these two new peaks merge into a single peak at 7.5 GHz in simulation and at 7.6 GHz in experiment, resulting in an absorption of only about 20%.

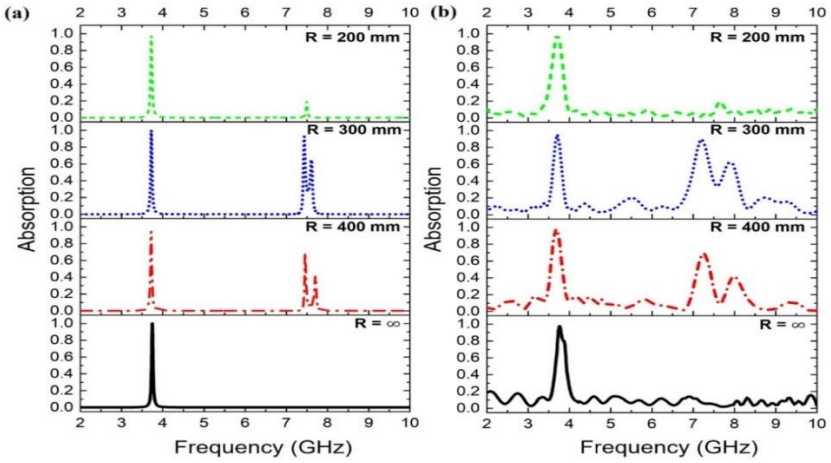

Figure 6. *(a) Simulated and (b) measured absorption spectra of the MPA with a decreasing bending radius from R = ∞ to R = 200 mm.*

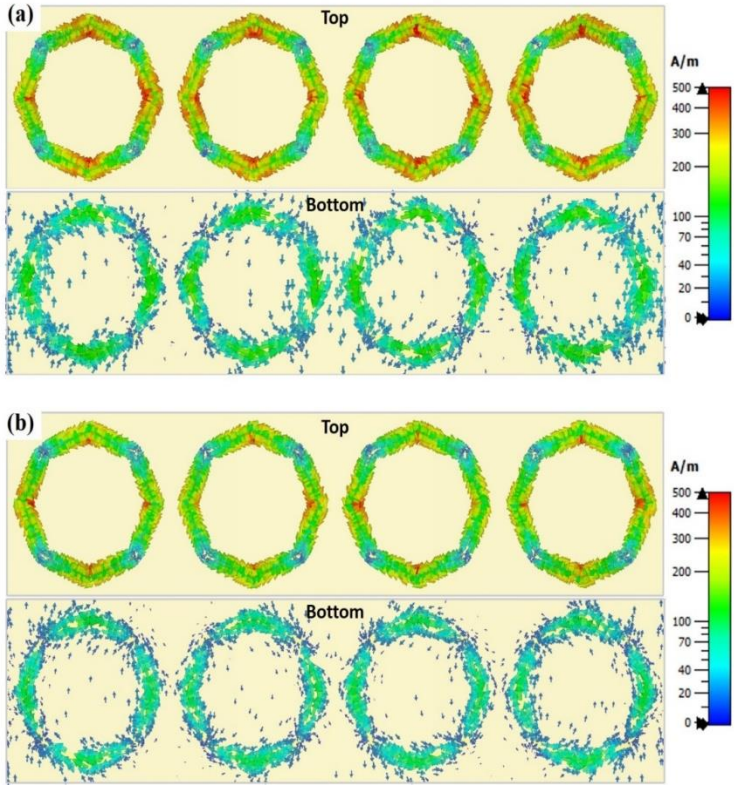

Figure 7. *Surface current distributions for the case of R = 300 mm at (a) 7.43 GHz and (b) 7.6 GHz*

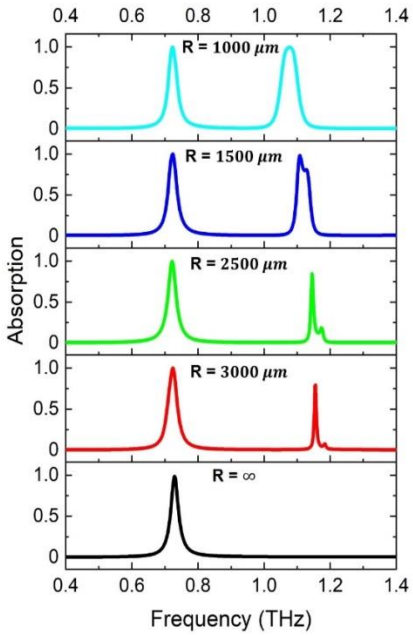

Figure 8. *Evolution of simulated absorption spectrum of the THz MPA when the bending radius is changed from R = ∞ (flat) to R = 1000 μm*

The distribution of surface current for the case of the bending radius, R = 300 mm, is presented in Figure 7. It can be observed that, strong surface currents are induced across all the unit cells at 7.43 GHz (Figure 7a) and 7.6 GHz (Figure 7b). However, the directions of induced currents at these two frequencies are antiphase. Additionally, on each unit cell, the surface currents are separated into two regions, where the induced currents are anti-parallel to each other. This phenomenon indicates that the new peaks at higher frequencies originate from second-order

magnetic resonance, which is caused by the bent state of the MPA structure, leading to an inhomogeneous distribution of electric and magnetic fields on the MPA surface [4], [5].

To further demonstrate the advantages of the proposed structural design, the suggested MPA is scaled down for operation in the THz region, and the structural parameters are listed in Table 1.

Table1. *Structural parameters of MPA design operating in the THz region*

Parameters	**p**	**r_1**	**r_2**	**t**
Values (μm)	100	45	35	5

The simulation results for controlling the absorption characteristics of the MPA within the THz region are presented in Figure 8. It is evident that the fundamental peak of the MPA, situated at approximately 0.73 THz with an absorption of 98.4%, remains largely unchanged during the transition from the flat state to various bent states, each characterized by distinct bending radii. Notably, the geometrical transition introduces two additional absorption peaks at higher frequencies. Specifically, when the bending radius is set at R = 3000 μm, two new peaks emerge at 1.15 THz (with an absorption of 80%) and 1.18 THz (with an absorption of 8.8%). Upon reducing the bending radius further, the absorption intensity of these two peaks escalates. Finally, when R = 1000 μm, these absorption peaks merge to form a single intense peak reaching a 99.5% absorption at 1.08 THz.at 1.08 THz. Concurrently, reducing the bending radius induces a slight shift of the additional absorption peaks toward lower frequencies. The operation of THz MPA is similar to that of the GHz MPA observed in the above discussion.

4. Conclusions

In this work, a mechanically-tunable metamaterial perfect absorber is investigated by both simulation and experiment. In the planar configuration, the proposed MPA exhibits a single-band absorption at 3.7 GHz with the absorption of 99.9% under normal incidence. The underlying mechanism of this perfect absorption peak is explained by the impedance matching between the structure and free space. At oblique incidences, high-order resonance peak is induced at frequency of 7.5 GHz for both TE and TM polarizations. Furthermore, as the proposed structure is bent with varying radii, the fundamental peak remains nearly constant, displaying an absorption of 99.9 % at 3.7 GHz. However, the behavior of the high-order absorption peaks changes significantly. When the bending radius decreases from $R = \infty$ to R = 300 mm, two new peaks emerge at higher frequencies, exhibiting absorption magnitudes of 92.6% (at 7.43 GHz) and 69% (at 7.6 GHz). Nevertheless, with a further decrease in the bending radius to R = 200 mm, these two new peaks merge into a single peak at 7.5 GHz with an absorption drops to 20%. Consequently, the proposed MPA can be characterized as single-band or triple-band, depending on mechanical deformation. The appearance of new peaks at high frequencies can be attributed to the excitation of high-order resonances induced by the asymmetric structure. In the end, the proposed MPA is scaled down to examine the mechanically-tunable characteristics in the THz region. In the flat configuration, the proposed structural design acts as a single-band MPA with an absorption peak at 0.73 THz (98.4% absorption). However, in the bending state, new peaks appear at higher frequencies, and the proposed MPA functions as a dual-band absorber. Our work might be used for expanding a new generation of tunable devices, especially, including filters, sensors and more, operating within the GHz and THz frequency ranges for the high technology farming.

Acknowledgements

This research is funded by Vietnam National Foundation for Science and Technology Development (NAFOSTED) under grant number 103.99-2020.23, and the Nippon Sheet Glass Foundation for Materials Science and Engineering.

REFERENCES

[1] N. I. Landy, S. Sajuyigbe, J. J. Mock, D. R. Smith, and W. J. Padilla, "Perfect Metamaterial Absorber," *Phys. Rev. Lett.*, vol. 100, no. 20, May 2008, Art. no. 207402.

[2] Z. Duan, X. Tang, Z. Wang, Y. Zhang, X. Chen, M. Chen, and Y. Gong, "Observation of the reversed Cherenkov radiation," *Nat. Commun.*, vol. 8, no. 1, Mar. 2017, Art. no. 14901.

[3] N. Seddon and T. Bearpark, "Observation of the Inverse Doppler Effect," *Science*, vol. 302, no. 5650, pp. 1537–1540, Nov. 2003.

[4] V. G. Veselago, "The electrodynamics of sbstances with simultaneously negative values of ε and μ," *Sov. Phys. Uspekhi*, vol. 10, no. 4, pp. 509–514, Apr. 1968.

[5] D. R. Smith, W. J. Padilla, D. C. Vier, S. C. Nemat-Nasser, and S. Schultz, "Composite Medium with Simultaneously Negative Permeability and Permittivity," *Phys. Rev. Lett.*, vol. 84, no. 18, pp. 4184–4187, May 2000.

[6] Y. I. Abdulkarima, L. Denga, H. Luoa, S. Huanga, M. Karaaslanc, O. Altıntas, M. Bakırd, F. F. Muhammadsharife, H. N.Awl, C.Sabah, and K. S. L. Al-badri, "Design and study of a metamaterial based sensor for the application of liquid chemicals detection," *J. Mater. Res. Technol.*, vol. 9, no. 5, pp. 10291–10304, Sep. 2020.

[7] L. Ma, D. Chen, W. Zheng, J. Li, S. Zahra, Y. Liu, Y. Zhou, Y. Huang, and G. Wen, "Advanced Electromagnetic Metamaterials for Temperature Sensing Applications," *Front. Phys.*, vol. 9, p. 657790, Apr. 2021.

[8] A. Sadeqi, H. R. Nejad, and S. Sonkusale, "Low-cost metamaterial-on-paper chemical sensor," *Opt. Express*, vol. 25, no. 14, Jul. 2017, Art. no. 16092.

[9] S. Haxha, F. AbdelMalek, F. Ouerghi, M. D. B. Charlton, A. Aggoun, and X. Fang, "Metamaterial Superlenses Operating at Visible Wavelength for Imaging Applications," *Sci. Rep.*, vol. 8, no. 1, Oct. 2018, Art. no. 16119.

[10] D. Shan, H. Wang, K. Cao, and J. Zhang, "Wireless power transfer system with enhanced efficiency by using frequency reconfigurable metamaterial," *Sci. Rep.*, vol. 12, no. 1, Jan. 2022, Art. no. 331.

[11] W.C. Harris and D. S. Ricketts, "Maximum gain enhancement in wireless power transfer using anisotropic metamaterials," *Sci Rep.*, vol.13, 2023, Art. no. 7726.

[12] G. P. E. Persis, J. J. Paul, T. B. Mary, and R. C. Joy, "A compact tilted split ring multiband metamaterial absorber for energy harvesting applications," *Mater. Today Proc.*, vol. 56, pp. 368–372, 2022.

[13] A. Elsharabasy, M. Bakr, and M. J. Deen, "Wide-angle, wide-band, polarization-insensitive metamaterial absorber for thermal energy harvesting," *Sci. Rep.*, vol. 10, no. 1, Oct. 2020, Art. no. 16215.

[14] K. Iwaszczuk, A. C. Strikwerda, K. Fan, X. Zhang, R. D. Averitt, and P. U. Jepsen, "Flexible metamaterial absorbers for stealth applications at terahertz frequencies," *Opt. Express*, vol. 20, no. 1, Jan. 2012, Art. no. 635.

[15] J. Kim, K. Han, and J. W. Hahn, "Selective dual-band metamaterial perfect absorber for infrared stealth technology," *Sci. Rep.*, vol. 7, no. 1, Jul. 2017, Art. no. 6740.

[16] D. Hu, T. Meng, H. Wang, Y. Ma, and Q. Zhu, "Ultra-narrow-band terahertz perfect metamaterial absorber for refractive index sensing application," *Results Phys.*, vol. 19, Dec. 2020, Art. no. 103567.

[17] Y. I. Abdulkarim, O. Altintas, A. S. Karim, H. N. Awl, F. F. Muhammadsharif, F. Ö. Alkurt, M. Bakir, B. Appasani, M. Karaaslan, and J. Dong, "Highly Sensitive Dual-Band Terahertz Metamaterial Absorber for Biomedical Applications: Simulation and Experiment," *ACS Omega*, vol. 7, no. 42, pp. 38094–38104, Oct. 2022.

[18] J.-F. Lv, C. Ding, F.-Y. Meng, J.-Q. Han, T. Jin, and Q. Wu, "A Tunable Metamaterial Absorber Based on Liquid Crystal with the Compact Unit cell and the Wideband Absorption," *Liq. Cryst.*, vol. 48, no. 10, pp. 1438–1447, Aug. 2021.

[19] M. Lei, N. Feng, Q. Wang, Y. Hao, S. Huang, and K. Bi, "Magnetically tunable metamaterial perfect absorber," *J. Appl. Phys.*, vol. 119, no. 24, Jun. 2016, Art. no. 244504.

[20] J. Ning, K. Chen, W. Zhao, J. Zhao, T. Jiang, and Y. Feng, "An Ultrathin Tunable Metamaterial Absorber for Lower Microwave Band Based on Magnetic Nanomaterial," *Nanomaterials*, vol. 12, no. 13, Jun. 2022, Art. no. 2135.

[21] Y. Shen, J. Zhang, Y. Pang, L. Zheng, J. Wang, H. Ma, and S. Qu, "Thermally Tunable Ultra-wideband Metamaterial Absorbers based on Three-dimensional Water-substrate construction," *Sci. Rep.*, vol. 8, no. 1, Mar. 2018, Art. no. 4423.

[22] T. Wu, W. Li, S. Chen, and J. Guan, "Wideband frequency tunable metamaterial absorber by splicing multiple tuning ranges," *Results Phys.*, vol. 20, Jan. 2021, Art. no. 103753.

[23] F. Zhang, S. Feng, K. Qiu, Z. Liu, Y. Fan, U̓. Zhang, Q. Zhao, and J. Zhou, "Mechanically stretchable and tunable metamaterial absorber," *Appl. Phys. Lett.*, vol. 106, no. 9, Mar. 2015, Art. no. 091907.

[24] J. Kim, H. Jeong, and S. Lim, "Mechanically actuated frequency reconfigurable metamaterial absorber," *Sens. Actuators Phys.*, vol. 299, Nov. 2019, Art. no. 111619.

[25] T. L. Pham, X. K. Bui, S. T. Bui, D. H. Le, V. L. Le, D. L. Vu, and T. T. Nguyen "Origami-based stretchable bi-functional metamaterials: reflector and broadband absorber," *J. Phys. Appl. Phys.*, vol. 54, no. 16, Apr. 2021, Art. no. 165111.

[26] 3DEXPERIENCE Company, "CST Studio suite electromagnetic field simulation software," [Online]. Available: https://www.3ds.com/products-services/simulia/products/cst-studio-suite/. [Accessed Nov. 1, 2023].

[27] S. Jung, Y. J. Kim, Y. J. Yoo, J. S. Hwang, B. X. Khuyen, L.-Y. Chen, and Y. P. Lee, "High-Order Resonance in a Multiband Metamaterial Absorber," *J. Electron. Mater.*, vol. 49, no. 3, pp. 1677–1688, Mar. 2020.

[28] X. Huang, C. Lu, C. Rong, Z. Hu, and M. Liu, "Multiband Ultrathin Polarization-Insensitive Terahertz Perfect Absorbers With Complementary Metamaterial and Resonator Based on High-Order Electric and Magnetic Resonances," *IEEE Photonics J.*, vol. 10, no. 6, pp. 1–11, Dec. 2018.

[29] Y. Cheng, Z. Cheng, X. Mao, and R. Gong, "Ultra-Thin Multi-Band Polarization-Insensitive Microwave Metamaterial Absorber Based on Multiple-Order Responses Using a Single Resonator Structure," *Materials*, vol. 10, no. 11, Oct. 2017, Art. no. 1241.

[30] J. S. Hwang, Y. J. Kim, Y. J. Yoo, K. W. Kim, J. Y. Rhee, L. Y. Chen, and Y. P. Lee, "Switching and extension of transmission response, based on bending metamaterials," *Sci. Rep.*, vol. 7, no. 1, Jun. 2017, Art. no. 3559.

[31] V. Aksyuk, B. Lahiri, G. Holland, and A. Centrone, "Near-field asymmetries in plasmonic resonators," *Nanoscale*, vol. 7, no. 8, pp. 3634–3644, 2015.